Sensitivity Analysis of Inverse Thermal Modeling to Determine Power Losses in Electrical Machines

Devi Geetha Nair[1], Paavo Rasilo[2], and Antero Arkkio[1]

[1]Department of Electrical Engineering and Automation, Aalto University, FI-00076 Espoo, Finland
[2]Laboratory of Electrical Energy Engineering, Tampere University of Technology, FI-33101 Tampere, Finland

Inverse analysis is a known mathematical approach, which has been used to solve physical problems of a particular nature. Nevertheless, it has seldom been applied directly for loss reconstruction of electrical machines. This paper aims to verify the accuracy of an inverse methodology used in mapping power loss distribution in an induction motor. Conjugate gradient method is used to iteratively find the unique inverse solution when simulated temperature measurement data are available. Realistic measurement situations are considered and the measurement errors corresponding to thermographic measurements and temperature sensor measurements are used to generate simulated numerical measurement data. An accurate 2-D finite-element thermal model of a 37 kW cage induction motor serves as the forward solution. The inverse model's objective is to map the power loss density in the motor accurately from noisy temperature measurements made on the motor housing's outer surface. Furthermore, the sensitivity of the adopted inverse methodology to variations in the number of available measurements is also considered. Filtering the applied noise to acceptable ranges is shown to improve the inverse mapping results.

Index Terms—**Heat transfer, induction motor, inverse problems.**

I. Introduction

MATHEMATICALLY and statistically based iron-loss models in rotating electrical machines aim to estimate losses both qualitatively and quantitatively. Nevertheless, various manufacturing defects and material peculiarities manifest, making measurements necessary to verify their accuracy. When models deviate from loss measurements, they are difficult to resolve, since certain machine parts are inaccessible to local measurements of temperature or flux density. Moreover, no-load measurement of core loss too is not always accurate; existing standards concern only sinusoidal voltage supply, whereas inverter supplied machines are on the rise [1].

The capability to measure local power loss in machines will be of considerable use and the concept of inverse thermal analysis is apt for the task, as it facilitates a body's unmeasurable heat losses to be determined from its measurable temperature rises. However, when the known temperatures are fewer than the unknown sources, the generally well-posed inverse heat problem becomes ill-posed. This causes the system to have many possible source solutions as opposed to a unique one. In addition, noise in measured temperature can also heavily destabilize it. Ill-posed problems are usually solved by "regularizing" or approximating them to a well-posed system through various means [2].

Inverse thermal methods in electrical machinery have much scope: in thermal parameter estimation, locating 3-D source from 2-D measurements and source strength determination from transient temperature measurements. Power loss in a 3-D volume of a current carrying bar was reconstructed from simulated surface thermographic measurements in [3]. Similarly, stator tooth losses in electrical motors were obtained from local temperature measurements in [4], albeit with some measurement inaccuracy. Time-dependent heat flux in the 3-D domain of a high-speed motor's housing is determined from its surface temperature in [5], through iterative steepest descent method. Other iterative and direct regularization methods have been studied in [6] and [7], respectively, to address inverse heat conduction problems in single-domain structures with simplistic geometries.

Inverse thermal mapping has mostly been restricted to singular domains of isotropic thermal properties. When multiple domains were considered, as in [3], they were "visible" also on the temperature measurement surface or boundary. In [5] and [6], the temperatures measured directly correspond to the heating surface's flux. These scenarios are relatively straightforward for inverse thermal mapping, since the measurement surfaces chosen are completely representative of the heat dynamics of the whole system. However, in rotating electrical machines such a characterization is difficult because of its complex structure. Moreover, there exist different power loss components that are generated in and propagated via conduction, convection, and radiation through the materials of different thermal properties. There is much scope for study here, and a detailed analysis still needs to be undertaken to choose the best inverse or optimization methodology to use with electrical motors as well as to assess its sensitivity to the number and nature of measurements.

In this paper, we present the possibility of applying the inverse approach to the whole machine such that all the heat sources are mapped, when all the intervening materials and modes of heat dissipation are considered. Thus far, inverse mapping has been applied at a lower scale, for simplistic cases. To address its applicability to a more complex scenario, this paper aims to reconstruct the power loss distribution throughout the whole 2-D motor geometry, from boundary temperatures. First, the forward problem of determining temperature distribution in the motor from volumetric power density is

Manuscript received March 16, 2018; revised April 27, 2018; accepted June 26, 2018. Corresponding author: D. G. Nair (e-mail: devi.nair@aalto.fi).
Color versions of one or more of the figures in this paper are available online at http://ieeexplore.ieee.org.
Digital Object Identifier 10.1109/TMAG.2018.2853084

TABLE I
TOTAL MEASURED AND COMPUTED ELECTRICAL LOSSES AND COMPONENTS OF COMPUTED LOSS AT DIFFERENT LOADS

Loading(Nm)	Iron loss* (W)		Copper loss* (W)		Total loss (W)	
	Stator	Rotor	Stator	Rotor	Compu.	Meas.
Full (237)	1215	912	542	171	2840	2945
Half (121)	368	199	478	132	1177	1182
No-load (1)	128	9	454	112	703	671

* Computed power loss components.

presented. The succeeding sections detail the inverse model and the choice of minimization technique used. In the interest of solution uniqueness, conjugate gradient (CG) method is used for inverse mapping, as opposed to constrained linear least squares in preceding studies [8]. The inverse model is tested for its accuracy in mapping heat flux, when simulated temperature data of the motor's frame (housing) is used. Each mesh node on the motor's frame is considered as a temperature measurement point with random measurement noise. Finally, the effect of number of measurements and measurement noise on numerical test data is discussed.

II. FORWARD THERMAL SOLUTION

The 37 kW induction motor's stator and rotor cores are stacks of radially laminated electrical steel sheets. They have a thermal conductivity of 28 W/mK in the radial and circumferential direction and a much lower conductivity of 0.6 W/mK in the axial direction. Hence, the majority of the heat dissipates outward toward the machine's housing, rather than axially to its end spaces. To obtain a temperature distribution faithful to the actual scenario of motor operation, 2-D numerical thermal analysis of the motor is carried out with power loss distribution as the source. A separate electromagnetic finite-element (FE) analysis of the motor generates the nodal power loss density in the 2-D cross section of the motor including the stator and rotor cores, slot windings and rotor bars. The accuracy of the electromagnetic loss computed this way was verified through measurements.

The motor's total loss was obtained from a temperature rise test following IEC 60034-2-1 standard. It is determined as the difference between the measured input power and the output power (measured from the torque transducer) at steady state. Once the motor reached steady state, the power was switched OFF, and the stator resistance was measured as a cooling down curve and extrapolated to the instant of power switch OFF. The average temperature of the stator winding was obtained from this resistance, which along with the measured stator current was used to calculate the stator resistive loss. Error analysis of the resistance measurement at full load (instrument error and extrapolation error) indicated the error limit to be ± 1.4 °C, which is not too high. Friction loss was measured separately through deceleration tests. The agreement between the computed and measured total electromagnetic loss was good and is shown in Table I.

The FE source distribution is then interpolated to the 2-D mesh of a sector of the motor's circular cross section

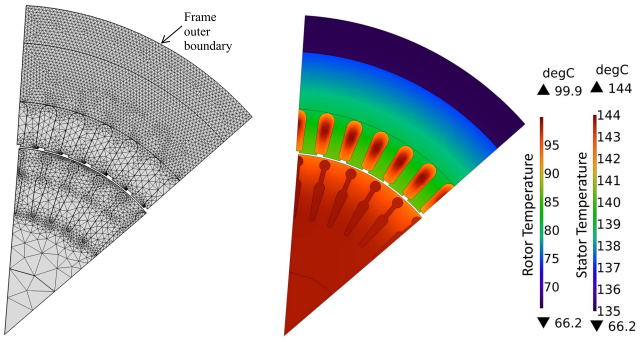

(a) (b)

Fig. 1. (a) 2-D mesh of the motor's cross section. (b) Steady-state temperature solution. Two legends: first referring to the rotor side and other to the stator side and frame.

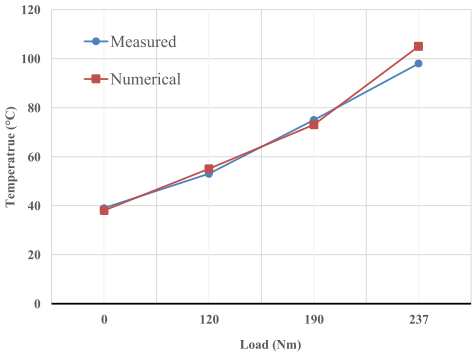

Fig. 2. Stator winding temperature: measured versus numerical results at different loads.

shown in Fig. 1(a). This is the model for further numerical thermal analysis. The forward thermal solution is the motor's temperature distribution obtained from the solution of the 2-D steady state forward thermal problem expressed as

$$\rho c_p \frac{\partial T}{\partial t} + \nabla \cdot q = Q_0. \tag{1}$$

The heat capacity of the material is established by ρ (denisty) and c_p (specific heat capacity). $q = -k\nabla T$ is the conductive heat flux, where k is the thermal conductivity of the medium and T is the temperature. Q_0 is the mapped volume power-loss density in W/m^3. Convection is imposed as Robin boundary conditions on the solid–fluid boundaries along the air gap and machine's frame. The convection thermal coefficients used were calibrated to match the temperatures measured at the stator end-winding, end spaces, and motor frame. The temperature distribution resulting from steady state analysis is shown in Fig. 1(b). The mean temperatures of regions match the measurements well. Fig. 2 indicates that the measured mean temperatures of the stator winding at different loads closely agree with those from the FE thermal analysis.

III. INVERSE THERMAL MODEL

The FE analysis of heat distribution in the motor is reduced to a system of linear equations, which in vector notation is

$$y = Ax. \tag{2}$$

Here, the nodal temperatures y are determined as linear combinations of different load (heat source) components x, as described by the system matrix A that is the linear operator. In terms of a thermal network, A is the thermal admittance matrix that quantifies the heat transfer between different regions. Thus, forward formulation solves for the nodal temperature y, provided the source x and other thermal parameters are known. On the other hand, the inverse problem aims to estimate the unknown source x, provided the temperature y is known. If all the temperatures are known accurately, the solution is straightforward and a unique solution can be found simply as $x = A^{-1}y$, which is known as the basic solution.

However, this formulation fails to return an acceptably accurate estimate of x if the known temperature data are not accurate. The temperatures are "known" through measurements, which always have errors. Thus, even if all the nodal temperatures are known from measurements y^{δ}, the resulting basic solution can be inaccurate. However, an approximate solution x_* can be found, for instance through constrained linear least square minimization as in [8] which satisfies

$$y^{\delta} \approx Ax_*. \tag{3}$$

The constraints forced the solution to be within the range of the true values and also stipulated that the sum of the elements equal the motor's total power loss. Here, x_* is the solution with the least residual $\|r\|$

$$\|r\| = \|Ax_* - y^{\delta}\|. \tag{4}$$

However, there can be more than one such solution which returns the least residual. In such cases, typically, the unique solution to the problem x_{k*} is the least residual solution $\|Ax_{k*} - y^{\delta}\|$ with minimum norm, $\min\|x_{k*}\|$. A set of solutions may be acceptable as possible causes behind a *desired* effect. However, there could be only one specific source solution which is the cause behind an *observed* effect. Therefore, uniqueness of inverse solution is important for electrical machines.

The initial point of the inverse formulation is the forward numerical thermal solution of the motor and forms the basis of the inverse mapping. The temperatures are assumed to be known (measured) on the frame boundary and the 2-D source distribution in the motor has to be found from this boundary data. Any available boundary measurement can be used, but here the frame or motor's housing is the chosen site of measurements, since it is the part most accessible and realistically available for non-invasive measurements in a fabricated motor. As indicated in the FE forward thermal solution, the frame section in contact with the stator core is of interest. The frame's outer boundary that is exposed to the ambient air is the boundary considered for measurements, as indicated in Fig. 1(a). The mesh node points here are chosen as the temperature measurement points. In the FE geometry, the actual ribbed frame was approximately modeled with a mean frame height.

To resemble measurements, noise of standard deviation σ is added to true nodal temperatures obtained on the outer frame boundary y_f, to give noisy measurements ${y_f}^{\delta}$. In addition, in order to simulate the real measurement scenarios where the instrument error can be compounded by other random measurement errors, a normally distributed random variable with zero mean, r_n is factored into the simulated measurement noise. This simulated measurement data ${y_f}^{\delta}$ with random measurement error are the given input to the inverse problem

$${y_f}^{\delta} = y_f + r_n\sigma. \tag{5}$$

The number of noisy measurements is $N({y_f}^{\delta}) = 70$. If this is the only known temperature data of the motor, it is rather challenging to find the heat source vector x_{k*}, where $N(x_{k*}) = 4368$. A fine mesh such as in Fig. 1(a) leads to strong linear dependencies causing noise in measurement to propagate and prevent a good inverse mapping. It is possible to employ direct regularization techniques like Tikhonov regularization here, but there is uncertainty regarding the optimal regularization parameter to use.

IV. Conjugate Gradient Method

CG method iteratively regularizes the inverse problem, so there is no need to identify regularizing parameters for the problem at the outset. Also, it is robust, with low computational cost when dealing with large matrices. It iteratively converges to the unique global minimum x_{k*} of the system when used with a suitable stopping criterion such as Morozov's discrepancy principle

$$\|y^{\delta} - Ax_*\| \leq \|\sqrt{N}\sigma\| \tag{6}$$

N being the number of measurement points, in this case 70. CG regularization with normal equations was carried out for the present FE system to solve for 4368 unknown sources from 70 noisy temperatures. However, the results were far from accurate. It was observed that the many intervening yoke and winding domains lead to loss of information across the material boundaries. Since the measurements are all on one boundary of the motor, computed heat fluxes are observed to get damped as we move further from the measurement surface.

Therefore, it is not possible to obtain loss distribution in the motor from frame measurements alone. A new temperature vector is assembled

$$y_m = \begin{bmatrix} {y_f}^{\delta} \\ y \end{bmatrix} \tag{7}$$

where y_m is the temperature vector used for inverse solution. It has the noisy frame temperatures ${y_f}^{\delta}$ but is augmented with the true forward temperature solution of the other nodes y. The system is now fully defined since $N(y_m) = 4368$ and an optimal source distribution x_{k*} can be found through CG. Iteration began from an initial assumption of zero nodal sources. The linear system A was preconditioned with a diagonal matrix composed of the diagonal elements of A, which reduced the solution time of CG.

The inverse mapped load vector x_{k*} is used as the new source (load vector) to the numerical model of the motor, and the steady state thermal problem is solved again. The flux distribution obtained thus is compared with the original, to identify any irregularities. The errors in the inverse reconstruction thus obtained are quantified in terms of maximum

and mean relative error

$$e_{\max} = \max\left(\left|\frac{x_{k*} - x}{x}\right|\right), \quad e_{\text{mean}} = \text{mean}\left(\left|\frac{x_{k*} - x}{x}\right|\right).$$

Another way of quantifying error is relative error norm

$$e_{\text{norm}} = \frac{\|x_{k*} - x\|}{\|x\|}.$$

While the mean relative error and relative error norm serve to denote the overall effectiveness of the inverse formulation, the maximum relative error is worth consideration, to understand the extent of the worst mapping and its repercussions.

A. Sensitivity Analysis

In order to evaluate the stability of the solution returned by CG, the noise level and the number of measurement points taken are varied. At steady state, the temperature along one circular perimeter of the motor's frame is mostly the same and was found to be 54.3 °C from the FE simulation. To account for the possible errors in temperature measurement, two feasible measurement scenarios for the frame are considered.

1) *Sensor Measurements:* This will resemble a situation where thermocouples or resistance temperature devices (RTDs) are placed on the frame. The lowest temperature measurement error is reportedly for Class A platinum RTDs, with an error of 0.35% in measuring 100 °C. Here, standard deviation of measurement error is $\sigma = 0.0035$.
2) *Thermal Camera Measurements:* Thermographic measurements using a thermal camera give the frame temperature distribution with a high resolution. The error in thermal camera measurements is 2%, so $\sigma = 0.02$.

Fig. 3 shows the total heat flux in the motor surface originally and with the reconstructed source vector. The variation is the most prominent along the frame boundary and along the stator teeth tips. The maximum heat flux in the motor originally is 10 048 W/m^2; with the reconstructed load vector, it is more than doubled, 25 900 W/m^2. However, this difference is dominant only in minor parts, as seen in Fig. 4.

Table II enumerates the difference between the expected and inverse mapped heat fluxes with the different error indicators mentioned earlier. The variation in this error with different numbers of measurement points at the two different noise levels is also shown. Owing to the ribbed structure of the frame, it is realistically not possible to fix RTD's in a tightly knit fashion resembling the measurement points on the mesh. Still, the comparison serves to shed light on the effect of measurement noise on inverse mapping's accuracy. The scenario with fewer number ($N = 30$) of non-adjacent measurement points, which is more in line with RTD measurements is considered also.

From the error margins, it is evident that the more the number of measurements considered, the higher the error. Fig. 4 shows the absolute difference in the original and mapped heat fluxes. The maximum relative variation is observed to be in the stator teeth tips. Nevertheless, the mean error in the overall mapping of the heat flux was not more than 4% at either noise levels.

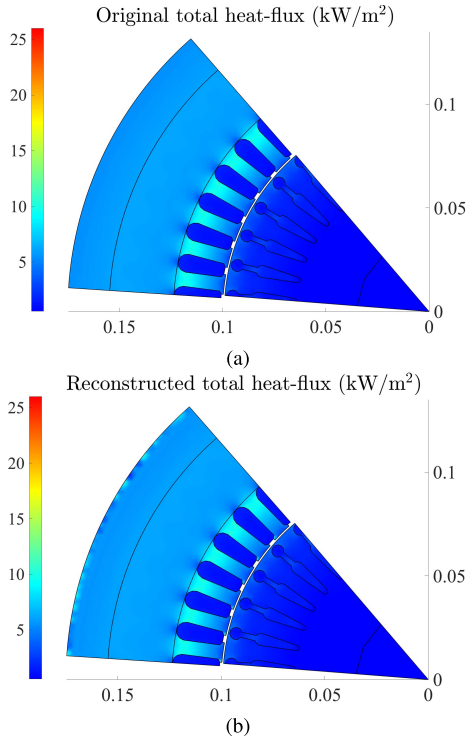

Fig. 3. (a) Original total flux distribution. (b) Total flux distribution with reconstructed source vector (70 measurement points, noise of $\sigma = 0.02$).

TABLE II
ERROR IN RECONSTRUCTION WHEN TWO DIFFERENT NOISE BOUNDS ARE USED FOR DIFFERENT NUMBER OF MEASUREMENT POINTS

Meas. Points	N = 70		N = 30		N = 1	
σ =	0.02	0.0035	0.02	0.0035	0.02	0.0035
e_{mean}%	3.7	0.5	2.3	0.36	0.3	0.04
$e_{\max}$%	639	86.2	683	69	66.4	7.8
e_{norm}%	22.6	2.6	14	1.9	1.8	0.2

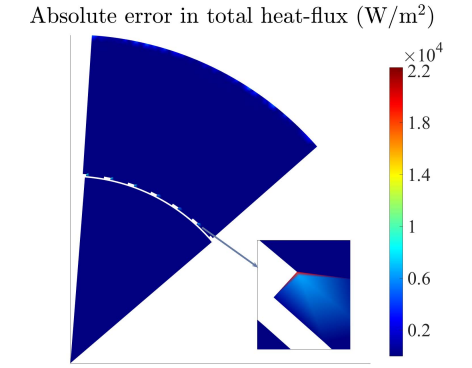

Fig. 4. Absolute error in heat flux mapping on the motor's surface. Enlarged region of the stator tooth shows that the maximum variation occurs here.

B. Need for Noise Smoothing

It is seen from the reconstruction in Figs. 3 and 4 that the inverse mapped heat flux varies from the original, particularly in the frame and tooth regions. The reason could be the highly fluctuating measured temperature data used. While temperature distribution can drastically change over material boundaries, within a domain of isotropic thermal conductivity such as the frame, the temperature change from node to node is gradual. Moreover, the frame boundary considered

TABLE III
ERROR IN INVERSE MAPPING AFTER NOISE SMOOTHING, FOR $\sigma = 0.02$

N	$e_{\text{mean}}\%$	$e_{\text{max}}\%$	$e_{\text{norm}}\%$
70	0.5	90	3
30	0.004	0.7	0.01

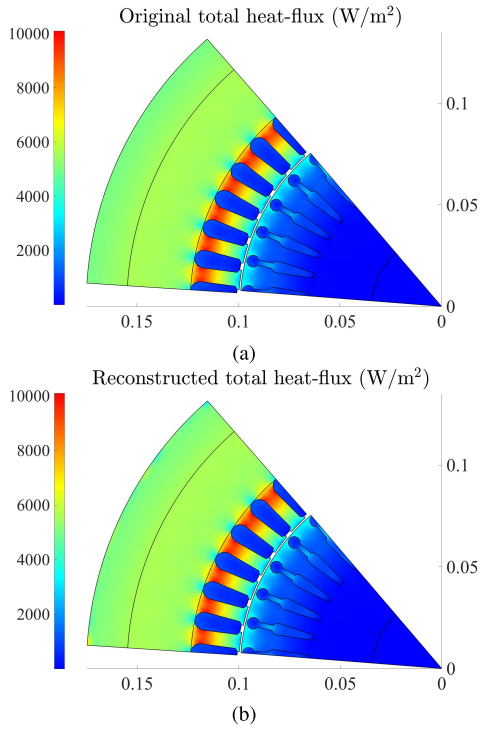

Fig. 5. (a) Original total flux distribution. (b) Total flux distribution with reconstructed source vector after smoothing ($N = 70$, noise of $\sigma = 0.02$).

for measurement is more or less isothermal. In such a case, the simulated random error imposed on the frame's measurement points has the effect of causing high variations in the temperatures from node to node on the same boundary. This is especially pronounced for $N = 70$ with $\sigma = 0.02$, where a higher noise bound caused high variation in temperature across adjacent nodes.

To counter this, the measurement error between adjacent nodes is filtered using a Gaussian function of a specified standard deviation. This approach was found to be suitable in [9] to improve the inverse power mapping at the microarchitectural level where the grid used was very dense. This approach to curbing high spatial variation was referred to as "smoothing" and is found to improve the inverse mapping. Table III lists the reduction in mapping error after noise smoothing was implemented.

The improvements are most pronounced in the case when $N = 70$. The same smoothing index trivializes the applied measurement error when $N = 30$, resulting in very low error margins. Since the measurement points here were nonadjacent, the variation in noise from one measurement point to another need not be suppressed to the same extent. A more relevant filter index needs to be used here, after observing the noise levels between the measurement points. Fig. 5 shows that the reconstructed flux after smoothing is well in the range of the original heat flux. The maximum variation, albeit lesser than before, was noted to be again in the teeth region.

V. DISCUSSION

Inverse power mapping in the motor's 2-D domain through iterative regularization with CG was not successful with only simulated measurements of frame boundary. Therefore, original surface temperature data from the rest of the domains were also used, to achieve a decent mapping accuracy. This became necessary since frame temperatures alone were insufficient to preserve the dynamics of heat transfer across different material boundaries. An improvement would be to consider measurements from additional, dissimilar boundaries and also few from motor domains. However, in a practical sense this would mean invasive measurements that are not always feasible in real scenarios. Hence, it has to be investigated further if isolated measurements of inner motor domains will augment boundary measurements enough to improve the regularized inverse solution. This is less likely in a dense mesh such as this one which represents the power distribution of the motor. Nevertheless, it is of use in inverse power mapping in a more discrete system, such as the motor's lumped thermal network.

Preconditioned CG converges fast and manages to effectively map the motor's heat flux. However, the maximum error in certain nodes was quite high. It was observed that the simulated measurement error caused high variations in temperature between adjacent measurement points. This is not realistic in a fine mesh; so high relative fluctuation in the simulated measured temperature across adjacent nodes is suppressed to a certain degree by filtering. With this, improved source fitting is achievable. Even without knowledge of the motor's original heat distribution, CG can still converge to the expected value.

ACKNOWLEDGMENT

This work was supported by the European Research Council under the European Union's Seventh Framework Programme (FP7/2007-2013)/ERC under Grant n°339380.

REFERENCES

[1] Z. Gmyrek, A. Boglietti, and A. Cavagnino, "Estimation of iron losses in induction motors: Calculation method, results, and analysis," *IEEE Trans. Ind. Electron.*, vol. 57, no. 1, pp. 161–171, Jan. 2010.

[2] M. J. Colaço, H. R. B. Orlande, and G. S. Dulikravich, "Inverse and optimization problems in heat transfer," *J. Brazilian Soc. Mech. Sci. Eng.*, vol. 28, no. 1, pp. 1–24, 2006.

[3] I. Marinova and V. Mateev, "Inverse source problem for thermal fields," *COMPEL-Int. J. Comput. Math. Elect. Electron. Eng.*, vol. 31, no. 3, pp. 996–1006, 2012.

[4] A. Krings, S. Nategh, O. Wallmark, and J. Soulard, "Local iron loss identification by thermal measurements on an outer-rotor permanent magnet synchronous machine," in *Proc. Int. Conf. Elect. Mach. Syst.*, 2012, pp. 1–5.

[5] C.-H. Huang and H.-C. Lo, "A three-dimensional inverse problem in estimating the internal heat flux of housing for high speed motors," *Appl. Thermal Eng.*, vol. 26, nos. 14–15, pp. 1515–1529, 2006.

[6] C.-H. Huang and C.-C. Tsai, "An inverse heat conduction problem of estimating boundary fluxes in an irregular domain with conjugate gradient method," *Heat Mass Transf.*, vol. 34, no. 1, pp. 47–54, 1998.

[7] A. Huhtala, S. Bossuyt, and A. Hannukainen, "*A priori* error estimate of the finite element solution to a Poisson inverse source problem," *Inverse Problems*, vol. 30, no. 8, p. 085007, 2014.

[8] D. G. Nair and A. Arkkio, "Inverse thermal modeling to determine power losses in induction motor," *IEEE Trans. Magn.*, vol. 53, no. 6, Jun. 2017, Art. no. 8103204.

[9] Z. Qi, B. H. Meyer, W. Huang, R. J. Ribando, K. Skadron, and M. R. Stan, "Temperature-to-power mapping," in *Proc. IEEE Int. Conf. Comput. Design*, Oct. 2010, pp. 384–389.